



Inhibition of ferroptosis promotes retina ganglion cell survival in experimental optic neuropathies

Miao Guo^{a,b,1}, Yanfang Zhu^{a,b,1}, Ying Shi^{a,b,c}, Xiangda Meng^{a,b}, Xue Dong^{a,b}, Haokun Zhang^{a,b}, Xiaohong Wang^{a,b,c,**}, Mei Du^{a,b,c,***}, Hua Yan^{a,b,d,*}

^a Department of Ophthalmology, Tianjin Medical University General Hospital, 300052, Tianjin, China

^b Laboratory of Molecular Ophthalmology and Tianjin Key Laboratory of Ocular Trauma, Tianjin Medical University, 300070, Tianjin, China

^c Department of Pharmacology and Tianjin Key Laboratory of Inflammation Biology, The Province and Ministry Co-sponsored Collaborative Innovation Center for Medical Epigenetics, School of Basic Medical Sciences, Tianjin Medical University, 300070, Tianjin, China

^d School of Medicine, Nankai University, 300071, Tianjin, China

ARTICLE INFO

Keywords:

Ferroptosis
Mitochondrial ROS
Glutathione peroxidase 4
Retinal ganglion cells
Optic neuropathies

ABSTRACT

Retinal ganglion cell (RGC) death is a hallmark of traumatic optic neuropathy, glaucoma, and other optic neuropathies that result in irreversible vision loss. However, therapeutic strategies for rescuing RGC loss still remain challenging, and the molecular mechanism underlying RGC loss has not been fully elucidated. Here, we highlight the role of ferroptosis, a non-apoptotic form of programmed cell death characterized by iron-dependent lethal lipid peroxides accumulation, in RGC death using an experimental model of glaucoma and optic nerve crush (ONC). ONC treatment resulted in significant downregulation of glutathione peroxidase 4 (GPx4) and system xc(−) cystine/glutamate antiporter (xCT) in the rat retina, accompanied by increased lipid peroxide and iron levels. The reduction of GPx4 expression in RGCs after ONC was confirmed by laser-capture microdissection and PCR. Transmission electron microscopy (TEM) revealed alterations in mitochondrial morphology, including increased membrane density and reduced mitochondrial cristae in RGCs after ONC. Notably, the ferroptosis inhibitor ferrostatin-1 (Fer-1) significantly promoted RGC survival and preserved retinal function in ONC and microbead-induced glaucoma mouse models. In addition, compared to the apoptosis inhibitor Z-VAD-FMK, Fer-1 showed better effect in rescuing RGCs death in ONC retinas. Mechanistically, we found the downregulation of GPx4 mainly occurred in the mitochondrial compartment, accompanied by increased mitochondrial reactive oxygen species (ROS) and lipid peroxides. The mitochondria-selective antioxidant MitoTEMPO attenuated RGC loss after ONC, implicating mitochondrial ROS and lipid peroxides as major mechanisms in ferroptosis-induced RGC death in ONC retinas. Notably, administering Fer-1 effectively prevented the production of mitochondrial lipid peroxides, the impairment of mitochondrial adenosine 5'-triphosphate (ATP) production, and the downregulation of mitochondrial genes, such as mt-Cytb and MT-ATP6, in ONC retinas. Our findings suggest that ferroptosis is a major form of regulated cell death for RGCs in experimental glaucoma and ONC models and suggesting targeting mitochondria-dependent ferroptosis as a protective strategy for RGC injuries in optic neuropathies.

1. Introduction

Retinal ganglion cells (RGCs) are the only projecting neurons within the retina that relay visual information from the retina to the brain [1,2]. The death of RGCs occurs in a variety of ocular diseases, including

traumatic optic neuropathy, glaucoma, and other optic neuropathies [3,4]. Like other central nervous system neurons in mammals, RGCs are devoid of replicative capabilities, and RGC loss often leads to irreversible vision loss and blindness [5,6]. Significant efforts have been made to find protective strategies to diminish or delay RGC death, including administering neurotrophic factors or inhibiting the apoptotic pathway

* Corresponding author. Tianjin Medical University General Hospital, No. 154, Anshan Road, Tianjin, 300052, China.

** Corresponding author. Tianjin Medical University, No. 22, Qixiangtai Road, Tianjin, 300070, China.

*** Corresponding author. Tianjin Medical University, No. 22, Qixiangtai Road, Tianjin, 300070, China.

E-mail addresses: xiaohongwang@tmu.edu.cn (X. Wang), dumei@tmu.edu.cn (M. Du), zyyanyan@tmu.edu.cn (H. Yan).

¹ Miao Guo and Yanfang Zhu contributed equally to this work.

Abbreviations	
AA	Arachidonic acid
ALA	α -linolenic acid
ATP	Adenosine 5'-triphosphate
BCA	Bicinchoninic acid
CC3	Cleaved caspase 3
cDNA	Complementary DNA
Cyto C	Cytochrome c
DAPI	4',6-diamidino-2-phenylindole
DEPC	Diethyl pyrocarbonate
DHA	Docosahexaenoic acid
DMSO	Dimethyl sulfoxide
DOX	Doxorubicin
EPA	Eicosapentaenoic acid
Fer-1	Ferrostatin-1
F-VEP	Flash visual evoked potentials
GAPDH	Glyceraldehyde-3-phosphate dehydrogenase
GPx4	Glutathione peroxidase 4
HE	Hematoxylin and eosin
HRMS/MS	High-resolution tandem mass spectrometry
IOP	Intraocular pressure
LA	Linoleic acid
MDA	Malondialdehyde
OD	Optical density
ONC	Optic nerve crush
PBS	Phosphate-buffered saline
PCR	Polymerase chain reaction
PFA	Paraformaldehyde
PVDF	Polyvinylidene difluoride
PUFAs	Polyunsaturated fatty acids
qRT-PCR	Quantitative real-time polymerase chain reaction
RBPMs	RNA binding protein with multiple splicing
RCD	Regulated cell death
RGCs	Retinal ganglion cells
RIPA	Radioimmunoprecipitation assay
RNFL	Retinal nerve fiber layer
ROS	Reactive oxygen species
RSL3	RAS-selective lethal
SD-OCT	Spectral-domain optical coherence tomography
TEM	Transmission electron microscopy
UHPLC	Ultra-high performance liquid chromatography
xCT	xc-cystine/glutamate antiporter

[7–9]. However, to date, no successful treatment has been approved for rescuing RGC loss. Therefore, a greater understanding of the mechanisms underlying RGC loss is urgently needed to develop effective treatment strategies.

Previous studies have demonstrated the existence of various forms of cell death, including apoptosis, autophagy, pyroptosis, and necrosis, in animal models of optic nerve axotomy, such as optic nerve transection or optic nerve crush (ONC) [9–14]. Among these, the role of autophagy in optic nerve damage remains controversial because some studies have reported cytoprotective effect of autophagy in promoting RGCs survival after traumatic injury [12], whereas others have shown detrimental effects of autophagy after optic nerve damage [10]. In contrast, substantial evidence supports apoptosis as the major mechanism leading to RGC death in animal models of optic nerve injury, experimental glaucoma, and in human glaucoma [9,15–18]. However, strategies targeting apoptotic pathways, including direct apoptosis inhibitors or activation of anti-apoptotic pathways, only result in partial neuroprotection in these models [19,20], suggesting that another form of cell death likely contributes to RGC loss in optic neuropathies. The molecular and cellular mechanisms that trigger RGC injury after optic nerve damage include oxidative stress, mitochondrial dysfunction, inflammation, and glutamate neurotoxicity [21–26]. Many of these risk factors are associated with ferroptosis, a recently recognized form of regulated cell death (RCD) [27–29]. However, the role of ferroptosis in optic neuropathies has been scarcely studied.

Ferroptosis was first proposed by Dixon et al. as a new form of programmed cell death, characterized by iron-dependent accumulation of lethal lipid oxidation [27]. Compared to other forms of RCD, such as apoptosis and necroptosis, ferroptosis exhibits distinct morphological, biochemical, and genetic features [27]. For example, unlike apoptosis, which is characterized by cell shrinkage or chromatin condensation, the key morphological hallmark of ferroptosis is mitochondrial shrinkage with increased membrane density and reduced mitochondrial cristae [27]. The iron-catalyzed Fenton reaction is thought to be critical for producing excessive lipid peroxides, leading to an imbalance in intracellular redox and, ultimately, cell death [30]. Therefore, molecules that disturb cellular redox homeostasis, such as erastin, induce ferroptosis, and iron-chelating agents can inhibit this process [29]. Ferroptosis is implicated in various pathophysiological conditions, including tumor suppression [31], ischemia/reperfusion injury [32], hereditary

hemochromatosis [33], and neurodegenerative disorders [34,35]. In the field of vision research, ferroptosis has been shown to occur in retinal pigment epithelial cells under oxidative stress or laser-induced choroidal neovascularization and photoreceptors after light-induced retinal degeneration [36–38]. Moreover, growing evidence supports the role of ferroptosis in neuronal injury in optic neuropathies. For example, previous studies have shown the accumulation of lipid peroxidation products in the trabecular meshwork and retina in experimental glaucoma models and glaucoma [39–42]. Furthermore, Sakamoto et al. reported that iron-chelating agents protected against excitotoxicity-induced neuronal injury in rat retinas [43].

The present study demonstrates, for the first time, that ferroptosis is the major form of RCD in RGC loss in an experimental model of glaucoma and ONC and that the ferroptosis inhibitor ferrostatin-1 (Fer-1) can promote RGC survival in these models by maintaining mitochondrial function. Our results offer new insights into the pathogenic mechanisms underlying RGC loss in optic neuropathies and may provide new targets for developing treatment strategies.

2. Results

2.1. Ferroptosis is involved in RGC injury in rats after ONC

To determine whether ferroptosis occurs in ONC-treated retinas, we examined the protein expressions of two key regulators of ferroptosis, glutathione peroxidase (GPx4) and system xc(–) cystine/glutamate antiporter (xCT) in rat retinas with or without ONC. Compared with control retinas, ONC retinas showed marked GPx4 and xCT down-regulation after one day of ONC that further decreased after three days of ONC (Fig. 1A, B, 1C). To explore whether these changes occur specifically in RGCs, RGCs were isolated using laser capture microdissection and mRNA expression of GPx4 in isolated RGCs were detected. Hematoxylin and eosin (HE) staining of retinal sections showed RGC layer captured before and after microdissection (Fig. 1D). Polymerase chain reaction (PCR) data showed that GPx4 levels were significantly down-regulated in isolated RGCs after three days of ONC treatment (Fig. 1E), supporting RGCs as the major site of ferroptosis induction in the retina after ONC. Furthermore, we found that the levels of malondialdehyde (MDA), an end-product of lipid peroxidation, were significantly increased in the retinas three days after ONC (Fig. 1F). The iron levels in

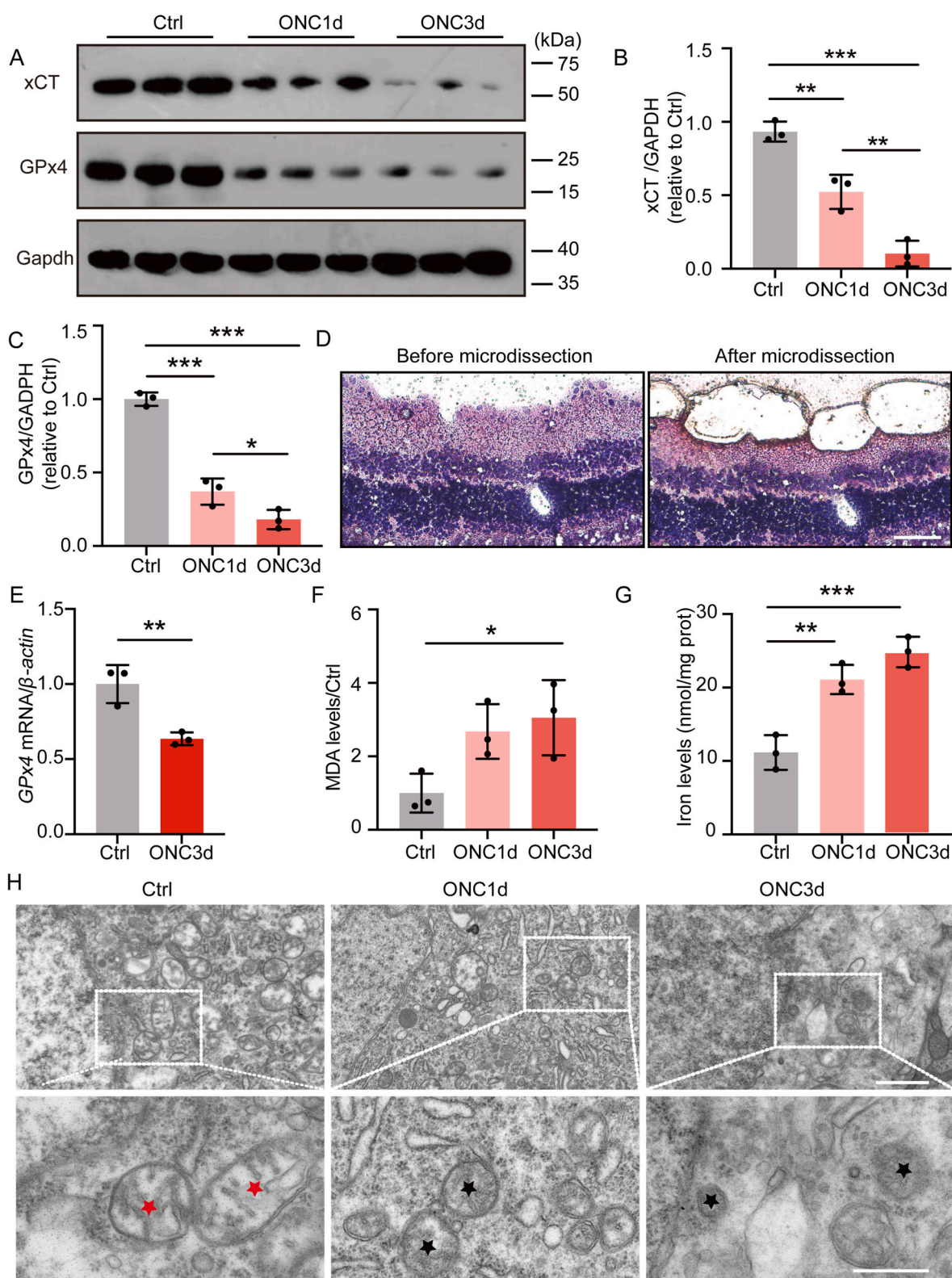


Fig. 1. Ferroptosis induction in rat retinas after ONC. (A–C) Western blot and densitometry analysis of xCT and GPx4 expression in retinas from control (ctrl) and ONC treated rats ($n = 3$ retinas per group). (D) HE staining of retinal sections before and after laser capture microdissection. (E) Detection of GPx4 mRNA expression in RGCs isolated by laser capture microdissection ($n = 3$ retinas per group). (F, G) Measurement of retinal MDA (F) and tissue iron (G) levels in control and ONC-treated retinas ($n = 3$ retinas per group). (H) Representative TEM images of retinal tissues with or without ONC treatment. The red and black asterisks indicate normal and shrunken mitochondria, respectively. All the results are expressed as the mean \pm SD; * $P < 0.05$, ** $P < 0.01$, and *** $P < 0.001$. Scale bars, 100 μm in (D), 1 μm (pictures above), and 500 nm (pictures below) in (H). (For interpretation of the references to colour in this figure legend, the reader is referred to the Web version of this article.)

the retinas after one and three days of ONC were significantly higher than those in the control group (Fig. 1G). Previous studies have reported distinct features of mitochondrial morphology in ferroptosis cells [27, 44]. Therefore, we examined the ultrastructure of mitochondria in RGCs one and three days after ONC using transmission electron microscopy (TEM). As shown in Fig. 1H, RGCs from ONC-treated retinas showed altered mitochondrial morphology compared to the control group. Specifically, we observed increased mitochondrial membrane density with reduced mitochondrial crista structures, consistent with the morphological features of mitochondria during ferroptosis reported previously [44].

In summary, the ONC treatment induced characteristic morphological and molecular changes in ferroptosis, including decreased GPx4 and xCT expression, increased lipid peroxidation and iron levels, and disruption of mitochondrial morphology in rat retinas, especially in RGCs.

2.2. Fer-1 effectively inhibits ferroptosis in rat retinas after ONC

As a lipid ROS scavenger, Fer-1 has been reported to inhibit ferroptosis in many studies [45,46]. In our study, high (1 mM) but not low (10 μ M) Fer-1 concentrations markedly restored GPx4 and xCT down-regulation in rat retinas three days after ONC (Fig. 2A, B, 2C). Additionally, Fer-1 treatment mitigated the increased MDA levels in the ONC retina (Fig. 2D). By using the ROS indicator dye CellROX Green, as previously reported [47], we observed elevated ROS levels in the RGC layer of rat retinas one day after ONC compared with control retinas, which can be prevented by treatment with 1 mM Fer-1 (Fig. 2E). Oxidation of polyunsaturated fatty acids (PUFAs) is the main driver of ferroptosis. Therefore, we used ultra-high performance liquid chromatography (UHPLC)-high-resolution tandem mass spectrometry (HRMS/MS) to measure the levels of PUFAs and oxylipins in the retina of ctrl, ONC and Fer-1-treated rats. We found that PUFA levels, including linoleic acid (LA), α -linolenic acid (ALA), and arachidonic acid (AA), were significantly increased in the retinas three days after ONC compared with control retinas (Fig. 2F). Further examination of retinal oxylipins revealed significantly higher levels of AA metabolites (11(12)-DiHET, 14(15)-DiHET, and 18-HETE (Fig. 2G)), eicosapentaenoic acid (EPA) metabolites (18-HEPE and 15-HpEPE (Fig. 2H)), and docosahexaenoic acid (DHA) metabolites (19(20)-DiHDPA, 19(20)-EpDPA, and 16(17)-EpDPA (Fig. 2J)) three days after ONC compared with controls. However, no significant difference in retinal LA metabolites was found between control and ONC rats (Fig. 2I). The Fer-1 treatment effectively mitigated the upregulation of these PUFAs and oxylipins in ONC-treated retinas (Fig. 2F, G, 2H, 2J).

Altogether, these data showed that Fer-1 effectively inhibited ferroptosis in ONC retinas.

2.3. Inhibition of ferroptosis by Fer-1 promotes RGC survival and improves flash visual evoked potential (F-VEP) function after ONC

To determine whether inhibiting ferroptosis could protect the retina from ONC-induced injuries, we examined retinal histology and retinal electrophysiology response after ONC. By immunostaining the retinas for the pan RGC marker, RNA binding protein with multiple splicing (RBPMS), we found that seven days of ONC treatment resulted in a 52% loss of RGCs compared to control retinas ($P < 0.001$). Additionally, treatment with Fer-1 (1 mM) significantly increased the number of RBPMS⁺ RGCs in ONC retinas to $64.5 \pm 5.8\%$ of that in control retinas ($P < 0.001$) (Fig. 3A and B), suggesting a protective effect of Fer-1 on RGC survival after ONC injury. Next, we measured the retinal thickness using optical coherence tomography (OCT) imaging and found that the thickness of the retinal nerve fiber layer (RNFL) significantly decreased after 14 days of ONC treatment. The Fer-1 treatment (1 mM) markedly mitigated the reduction in RNFL thickness (Fig. 3C and D). To determine whether preservation of RGCs numbers by Fer-1 could also restore the

visual function, we measured the F-VEP responses in ONC retinas to evaluate the visual responses of the retina and the optic pathway. Fig. 3E shows the representative waveforms of the F-VEPs for each group. It showed that ONC for seven days significantly reduced the amplitudes of N1P1 from 13.0 ± 2.5 μ v to 4.9 ± 0.7 μ v, and P1N2 from 16.5 ± 2.2 μ v to 3.4 ± 0.9 μ v. The Fer-1 treatment markedly restored the amplitudes of N1P1 and P1N2 to 9.1 ± 2.5 μ v and 7.8 ± 0.9 μ v, respectively (Fig. 3F and G). Furthermore, Fer-1 significantly shortened the prolonged latencies of N1 (78.8 ± 19.8 ms) and P1 (125.3 ± 30.0 ms) caused by ONC injury (N1 = 45 ± 3.9 ms, P1 = 73.8 ± 7.5 ms, $P < 0.01$) (Fig. 3H and I).

In conclusion, in ONC eyes, inhibition of ferroptosis by Fer-1 not only promoted RGC survival and preserved the retinal integrity, but also greatly improved visual function.

2.4. Fer-1 promotes RGC survival and preserves the retinal structure in a mouse model of glaucoma

To investigate whether ferroptosis contributes to RGCs injury in glaucoma, a microbeads injection-induced glaucoma mouse model as previously reported was used in this study [48,49]. Compared to saline-injected eyes, injection of microbeads into the anterior chamber of the mice caused elevation of the intraocular pressure (IOP) from basal levels of 12.9 mmHg–22.7 mmHg three days after injection. They remained elevated until day 21 (Fig. 4A). Concomitantly, microbead-injected eyes showed decreased RGC density and reduced RNFL thickness in the retina 28 days after the microbead injection (Fig. 4D–G). To examine ferroptosis induction in this glaucoma model, we measured the protein expression of the ferroptosis regulator GPx4 in the retina after microbead injection. GPx4 expression was significantly reduced in the retina of microbead-injected eyes compared to saline-control eyes 28 days later (Fig. 4B and C). The Fer-1 pretreatment before injecting the microbeads restored the decreased GPx4 protein expression without affecting elevated microbead-induced IOP (Fig. 4A, B, 4C). Furthermore, pretreating the samples with Fer-1 promoted RGC survival from $2458 \pm 125/\text{mm}^2$ to $3009 \pm 105/\text{mm}^2$ in the retinas of microbead-injected eyes (Fig. 4E) and markedly prevented the reduction in RNFL thickness caused by the microbead injection (Fig. 4F and G).

In summary, our data showed that inhibiting ferroptosis could protect against retinal injuries in a microbead injection-induced glaucoma mouse model.

2.5. Ferroptosis is the major form of RCD in RGCs after ONC injuries

Previous studies have shown an important role of apoptosis in RGCs death after ONC [20]. To investigate the significance of ferroptosis in comparison to apoptosis in ONC-induced RGCs death, we examined the time-course expression of the ferroptosis marker GPx4 and the apoptosis markers cleaved caspase-3 (CC3) and cytochrome c (Cyto C), which are released into the cytosol to activate mitochondria-dependent apoptosis. We found that the expression of CC3 significantly increased three days after ONC (Fig. 5A and B), while Cyto C significantly increased one day after ONC and remained high thereafter (Fig. 5A and C). In contrast, GPx4 levels were downregulated as early as 6 h after ONC treatment (Fig. 5A and D), accompanied by increased accumulation of the lipid peroxidation product MDA (Fig. 5H), suggesting that ferroptosis is an early event in the rat retina after ONC in comparison to apoptosis. Besides, applying Fer-1 after ONC did not prevent caspase-3 activation in rat retinas seven days after ONC (Fig. 5E and F), suggesting that ferroptosis occurs independently of apoptosis in ONC-treated retinas.

To investigate the relative contributions of ferroptosis and apoptosis in RGCs death after ONC, we compared the effects between ferroptosis and apoptosis inhibitor, as well as the combination of both inhibitors, in ONC treated rat retinas. Injection of the apoptosis inhibitor Z-VAD-FMK (Z-VAD) (400 ng) into the vitreous before and three days after ONC effectively blocked the release of Cyto c into the cytosol at seven days after ONC (Fig. 5G and I). We evaluated RGC survival (RBPMS⁺ cells) in

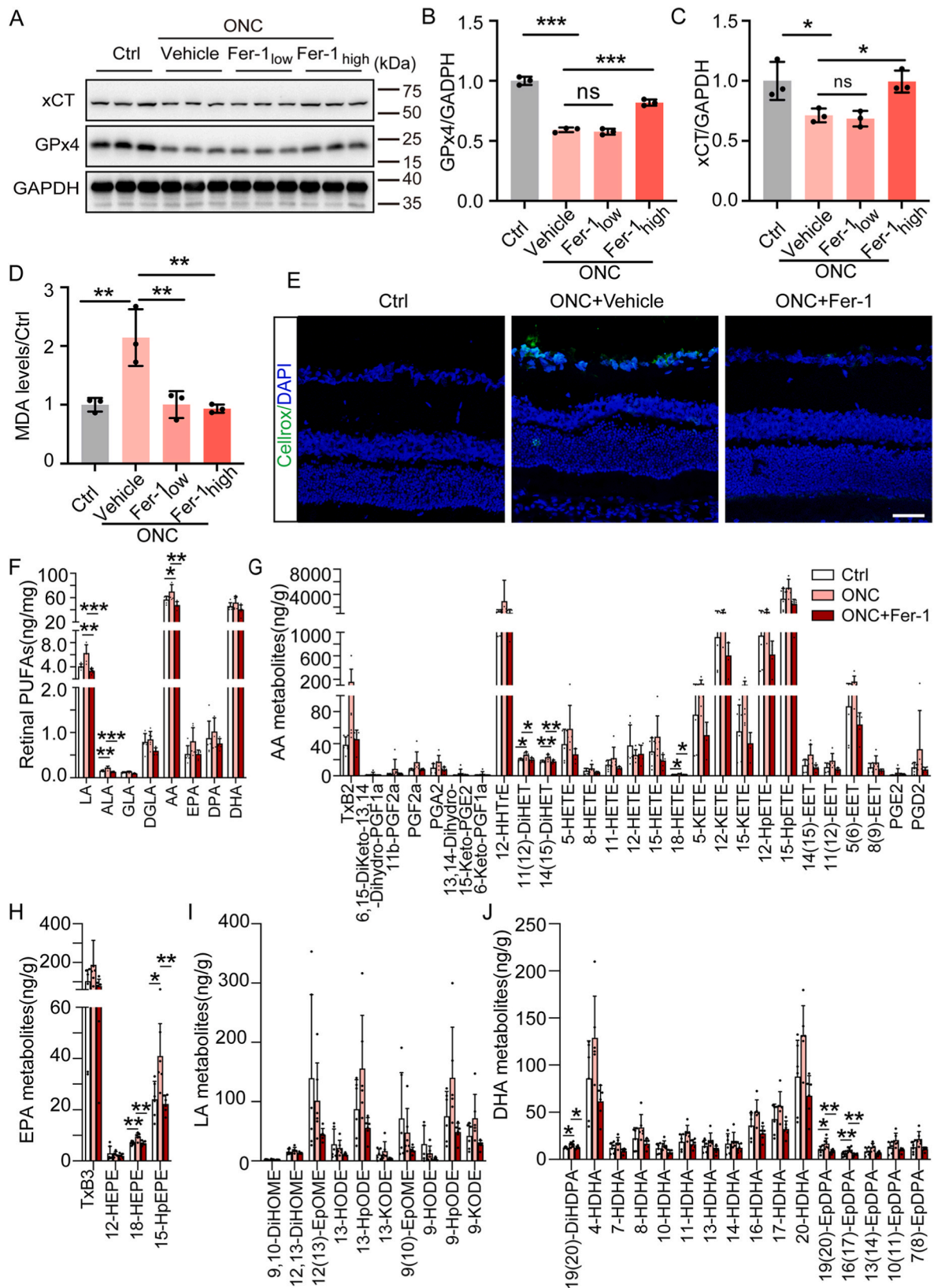


Fig. 2. Fer-1 effectively inhibits ferroptosis in rat retinas following ONC. (A–C) Western blot and densitometry analysis of xCT and GPx4 expression in control retinas and retinas after three days of ONC treated with or without Fer-1 (low = 10 μM, high = 1 mM) (n = 3 retinas per group). (D) Measurement of retinal MDA levels in control rats and rats after three days of ONC treated with or without Fer-1 (n = 3 retinas per group). (E) Representative images of CellROX staining in retinas from control rats and rats after one day of ONC treated with or without Fer-1 (n = 3 retinas per group). (F–J) Summary of retinal PUFAs (F) and AA (G), EPA (H), LA (I), and DHA metabolites (J) in control rats and rats after three days of ONC treated with or without Fer-1 (n = 3–6 retinas per group). The data are expressed as the mean ± SD. *P < 0.05, **P < 0.01, and ***P < 0.001. Scale bars, 50 μm in (E).

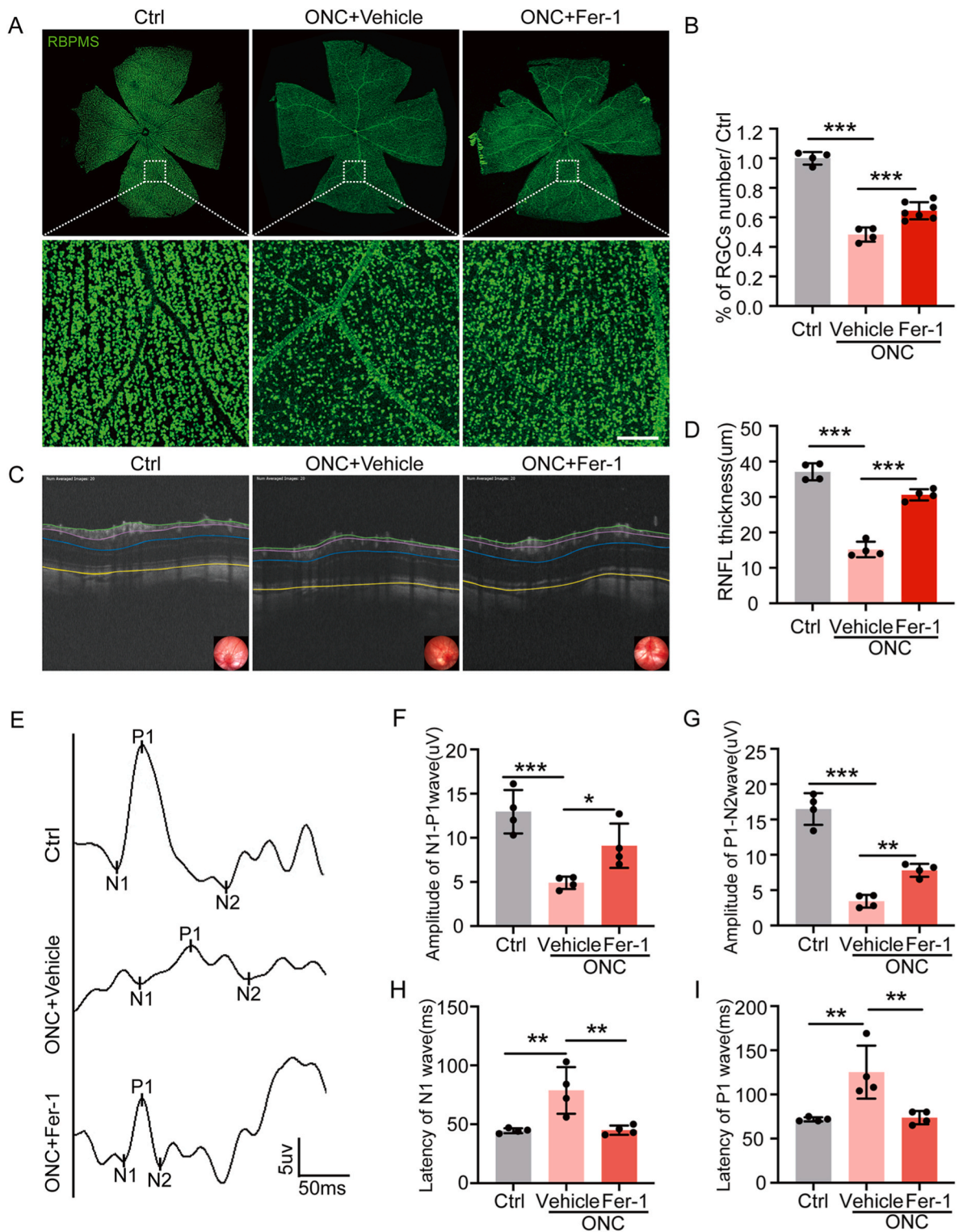


Fig. 3. Fer-1 protects against RGC loss, the reduction of retinal thickness, and the impairment of retinal function caused by ONC. (A) Retinal wholemount staining of RBPMS⁺ RGCs from control rats and rats after seven days ONC treated with or without Fer-1. (B) Quantification of RBPMS⁺ RGCs shown in (A) (n = 4–7 retinas per group). (C) Representative OCT images along a circle centered on the optic disc of the retina with a circumference of 3600 μm (the black circle in the Fundus photograph) from control rats and rats after 14 days of ONC treated with or without Fer-1. (D) Quantification of the mean RNFL thickness of the retina shown in (C) (n = 4 retinas per group). (E) Representative F-VEP responses from control, seven days post-ONC, and Fer-1-treated ONC eyes. (F–I) Quantification of the amplitudes of N1–P1, P1–N2, and the latencies of the N1 and P1 wave (n = 4 retinas per group). The data represent the mean ± SD. *P < 0.05, **P < 0.01, and ***P < 0.001. Scale bar, 200 μm in (A).

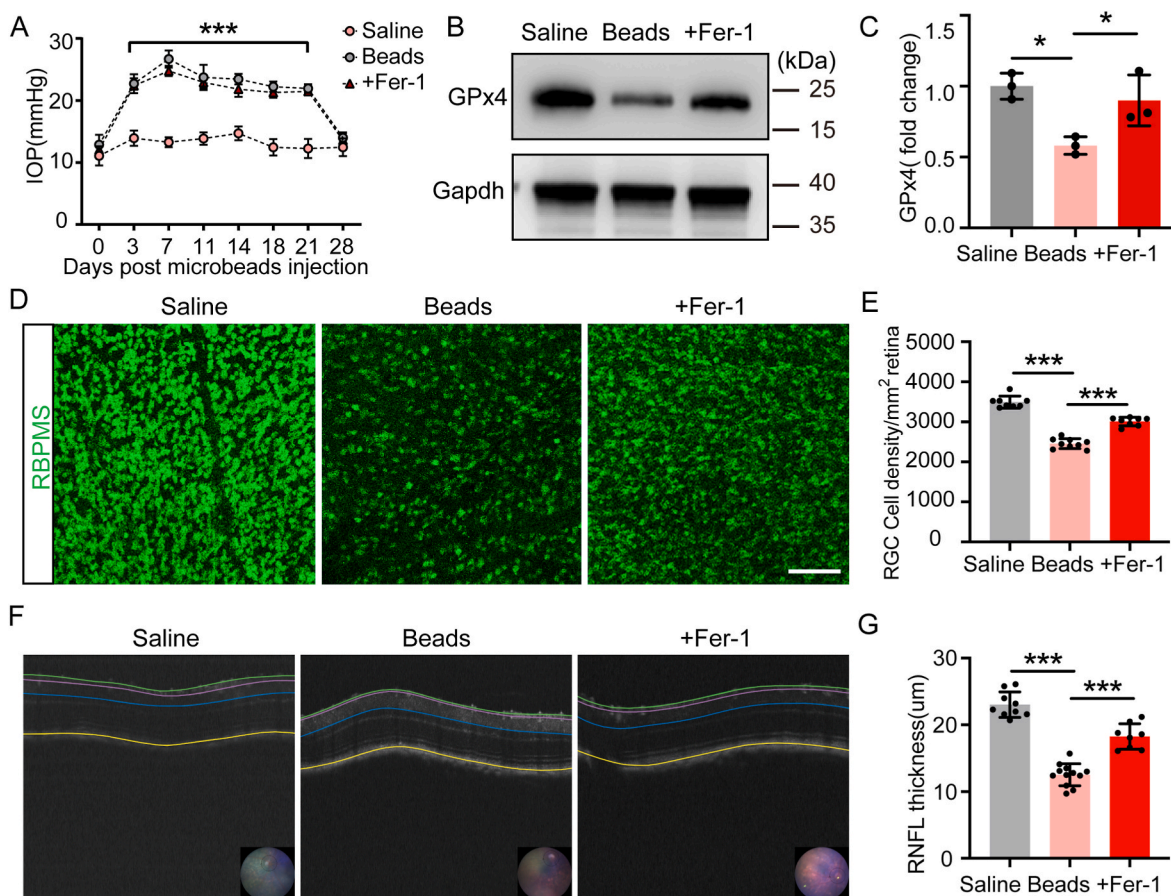


Fig. 4. Fer-1 protects against RGC injury in a microbead injection-induced glaucoma mouse model. (A) Measurement of IOP in mice after the microbead injection up to 28 days ($n = 8-15$ retinas per group). (B, C) Western blot and densitometry analyses of GPx4 expression in retinas 28 days after saline- and microbead-injected mice pretreated with or without Fer-1 ($n = 3$ retinas per group). (D) Retinal wholemount labeling of RBPMS⁺ RGCs isolated from saline- or microbead-injected eyes treated with or without Fer-1 28 days post-injection. (E) Quantification of RBPMS⁺ RGCs shown in (D) ($n = 8-9$ retinas per group). (F) Representative OCT images of retinas from saline- or microbead-injected mice 28 days post-injection. (G) Quantification of the mean RNFL thickness shown in (F) ($n = 9-13$ retinas per group). The data represent the mean \pm SD. * $P < 0.05$ and *** $P < 0.001$. Scale bar, 100 μ m in (D).

retinal wholemounts seven days after ONC and found that treatment with Z-VAD or Fer-1 markedly preserved RGC numbers (Fig. 5J). Specifically, compared to ONC alone group, the survival rate of RGCs in ONC retinas treated with Z-VAD, Fer-1, or dual inhibitors increased from $48.9\% \pm 6.3\%$ – $59.8\% \pm 1.4\%$, $67.1\% \pm 2.3\%$, and $76.4\% \pm 7.3\%$, respectively (Fig. 5K), suggesting that dual inhibitors showed a better effect in rescuing RGCs than either inhibitor alone.

Similarly, OCT measurements of retinal structure 14 days after ONC revealed that Z-VAD, Fer-1, or dual inhibitors significantly prevented the reduction in retinal thickness, especially at the RNFL (Fig. 5L). Among these, Fer-1 worked better than Z-VAD in protecting the retinal structure, and the combination of Fer-1 and Z-VAD conferred additive protection of the retinal structure compared to either inhibitor alone (Fig. 5M).

Collectively, these data demonstrate that ferroptosis, along with apoptosis, is the dominant form of RCD that contributes to RGC death in rat ONC models.

2.6. Fer-1 protects against ONC-induced RGC injury by maintaining mitochondrial function

Changes in mitochondrial morphology and function are closely related to ferroptosis, and recent studies have shown that mitochondrial dysfunction can be a causative factor in ferroptosis [50,51]. To investigate whether this also occurs in the retina after ONC, we first detected mitochondrial ROS production using the mitochondrial superoxide

indicator MitoSOXTM red. We found mitochondrial ROS was significantly increased in the RGC layer one day after ONC (Fig. 6A and B). Intravitreal injection of MitoTEMPO, a mitochondria-targeted ROS scavenger, effectively abolished mitochondrial ROS generation in RGCs of ONC retinas. Interestingly, like MitoTEMPO, the Fer-1 treatment also effectively reduced mitochondrial ROS in ONC retinas (Fig. 6A and B). Moreover, the Fer-1 treatment effectively mitigated the downregulation of mitochondrial genes mt-Cytb and MT-ATP6 in the retina three days after ONC (Fig. 6C and D). Treatment with either MitoTEMPO or Fer-1 effectively alleviated the reduction in adenosine 5'-triphosphate (ATP) production in the retina one day after ONC (Fig. 6E), suggesting a protective effect of Fer-1 in maintaining mitochondrial function after ONC injury.

GPx4 acts as the main regulator of ferroptosis by exerting its unique function of reducing lipid ROS production. To understand the role of mitochondrial form of GPx4 (mGPx4) in ONC-induced ferroptosis in the retina, we isolated the mitochondrial fraction of the retina, and found that mGPx4 expression was significantly decreased in the retina as early as 6 h after ONC injury, and continued to decrease until seven days after ONC, while GPx4 expression in the cytoplasmic fraction of ONC retina was not considerably affected (Fig. 6F–I), indicating that GPx4 expression in mitochondrial compartment might be affected initially after ONC treatment. Concomitantly, MDA levels were significantly increased in the mitochondrial fraction from 6 h to three days after ONC, but no significant change of MDA levels was found in the cytoplasmic fraction at the observed time points (Fig. 6J and K). These data suggest that

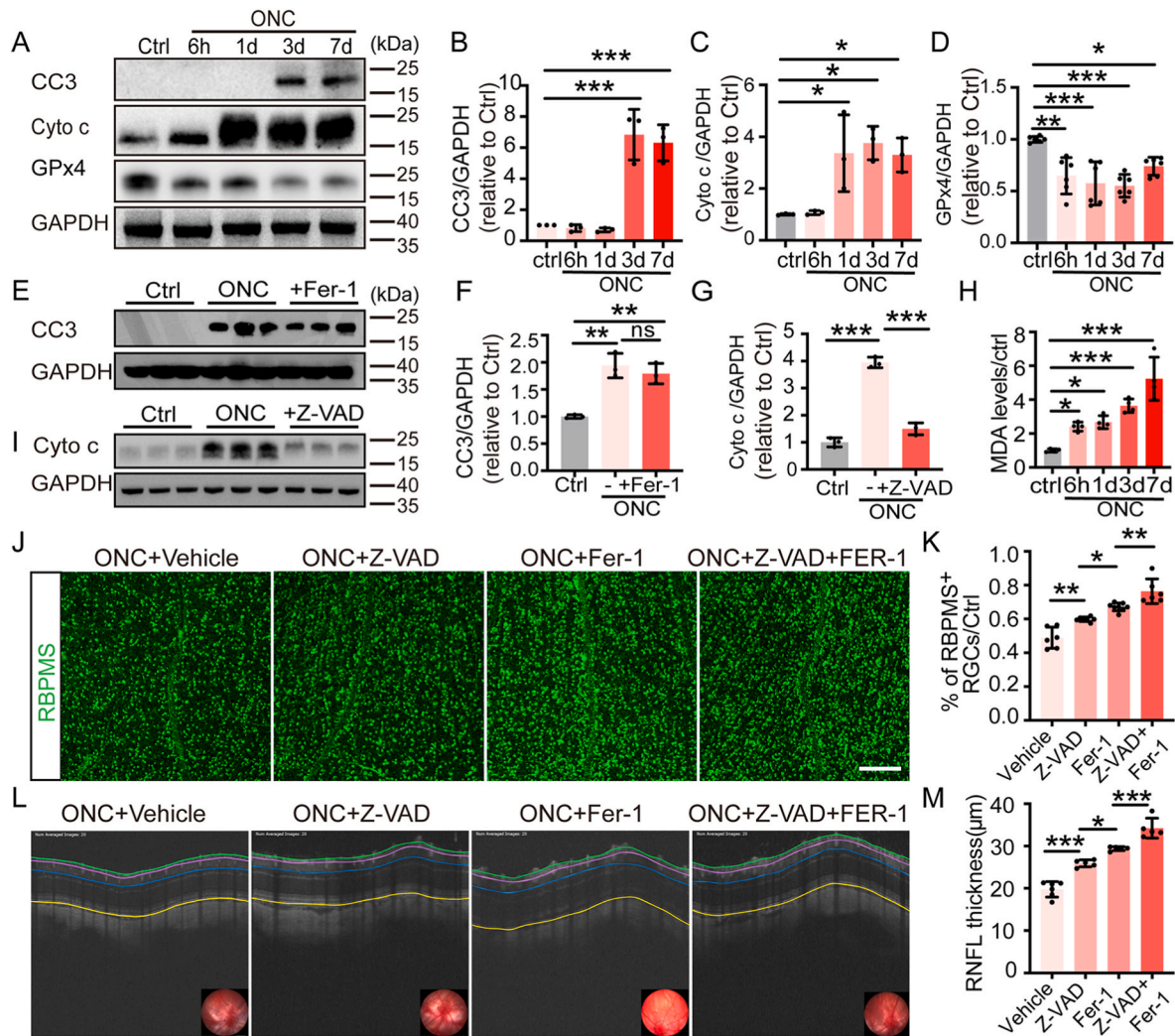


Fig. 5. Ferroptosis is the main form of RCD in ONC-induced RGC injury. (A–D) Western blot and densitometry analysis of cleaved caspase 3 (CC3), cytochrome *c* (Cyto C), and GPx4 expression in retinas after ONC for the indicated time ($n = 3–6$ retinas per group). (E, F) Western blot and densitometry analysis of cleaved caspase 3 in control, seven days post-ONC, and Fer-1-treated ONC retinas ($n = 3$ retinas per group). (G and I) Western blot and densitometry analysis of Cyto C in control, seven days post-ONC, and Z-VAD-FMK-treated ONC retinas ($n = 3$ retinas per group). (H) Measurement of MDA levels in retinas after ONC for the indicated time ($n = 4$ retinas per group). (J) Retina wholemount labeling of RBPMS⁺ RGCs following seven days of ONC with or without Fer-1 or Z-VAD treatment. (K) Quantification of RBPMS⁺ RGCs shown in (J) ($n = 6–8$ retinas per group). (L) Representative OCT images of retinas from control rats and rats after 14 days of ONC injury treated with or without Fer-1 or Z-VAD. (M) Quantification of the RNFL thickness of the retina shown in (L) ($n = 5–6$ retinas per group). The data represent the mean \pm SD. * $P < 0.05$, ** $P < 0.01$, and *** $P < 0.001$. Scale bars, 200 μ m in (J).

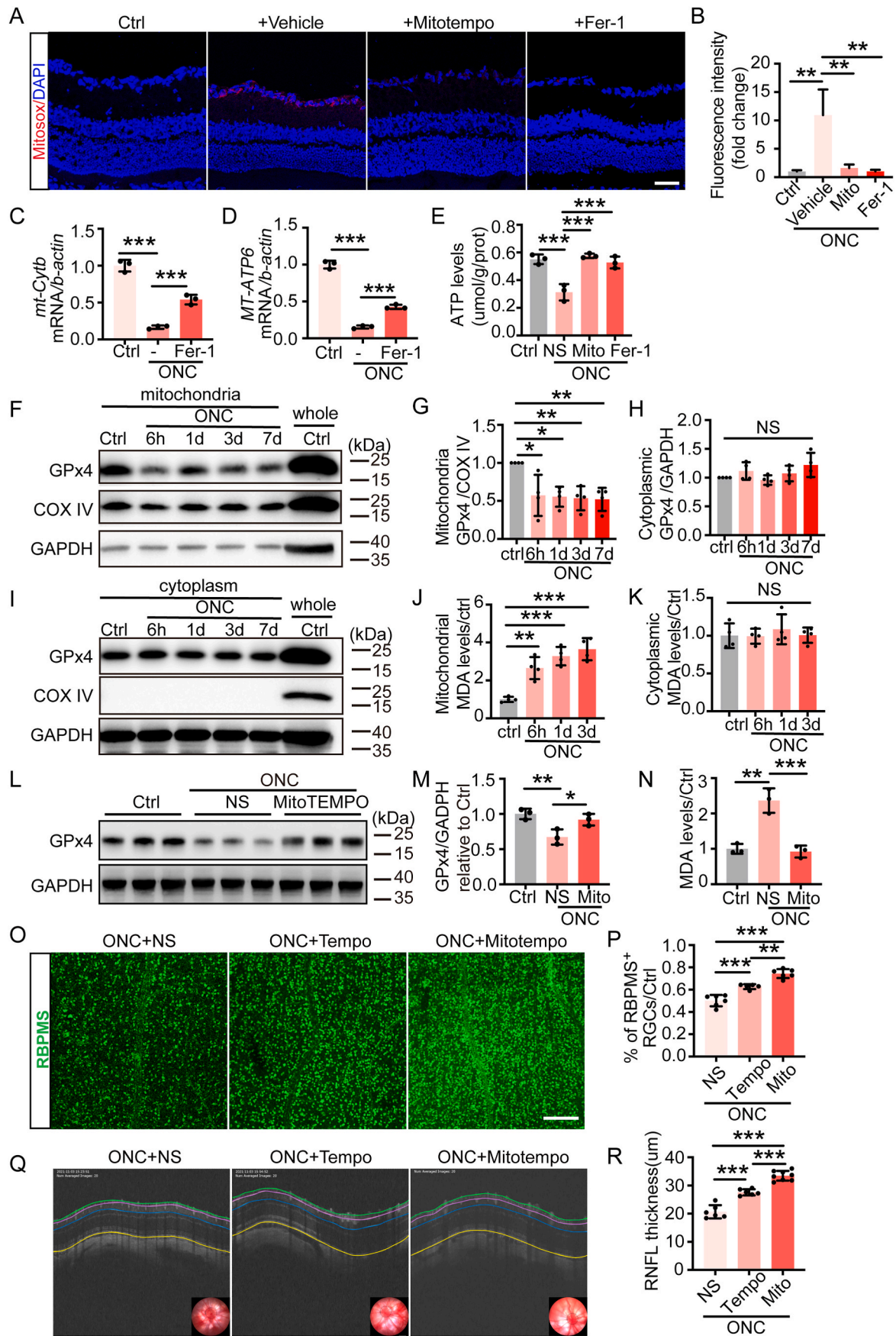
mitochondria compartment was primarily affected after ONC treatment and mitochondria ROS and lipid peroxides might trigger ferroptosis in ONC retinas. To further test this possibility, we injected MitoTEMPO into the vitreous of the ONC rats, and found that MitoTEMPO dramatically ameliorated GPx4 protein reduction and prevented MDA accumulation in the retina three days after ONC (Fig. 6L–N). Furthermore, by labeling RBPMS⁺ RGCs in retina wholemount and measuring RNFL thickness seven days and 14 days after ONC, respectively, we found that at seven days after ONC, the number of surviving RGCs was markedly increased in TEMPO (62.8%) and MitoTEMPO (74.5%) treatment group compared to surviving RGCs (50.2%) in the control group, with MitoTEMPO showing a significantly improved effect than TEMPO in preserving RGC survival ($P = 0.002$). Besides, the RNFL thickness was also well preserved in TEMPO and MitoTEMPO treated retinas compared to control retinas (Fig. 6O–R).

Altogether, these data implicate mitochondrial ROS and lipid peroxides as causative factors in ONC-induced ferroptosis and RGC death. Fer-1 could alleviate ONC-induced retinal injuries by ameliorating these mitochondrial deficits.

3. Discussion

RGC degeneration is a hallmark of glaucoma and other optic neuropathies that afflict millions of people worldwide [52]. However, neuroprotective therapies that diminish or delay the progression of RGC loss still remain a major clinical challenge. In the current study, we demonstrated that ferroptosis is an important mediator of RGC death in an ONC rat model and in a microbead injection-induced glaucoma mouse model. Notably, utilizing the ferroptosis inhibitor Fer-1 effectively alleviated RGC death, preserved retinal structure, and improved visual function in these models. Mechanistically, we revealed that mitochondrial dysfunction, particularly the accumulation of mitochondrial ROS and lipid peroxides, is essential for triggering ferroptosis in the rat retina after optic nerve damage.

The mechanisms underlying RGC death in optic neuropathies have not been fully elucidated and remain a matter of intense research. Previous studies have reported the involvement of different forms of cell death, including apoptosis, pyroptosis, and necrosis, in animal models of optic nerve damage [9–14]. However, inhibiting either apoptosis or



(caption on next page)

Fig. 6. Mitochondrial ROS and lipid peroxidation are crucial in ONC-induced ferroptosis and RGC loss. (A, B) Representative MitoSox images and quantification of the immunofluorescence intensity in retinas from control, one day post-ONC, and ONC treated with MitoTEMPO or Fer-1 rats ($n = 3$ retinas per group). (C, D) Detection of mt-Cytb (C) and MT-ATP6 (D) mRNA expression by qRT-PCR in control, three days post-ONC, and Fer-1-treated ONC retinas ($n = 3$ retinas per group). (E) Measurement of retinal ATP levels in control, one day post-ONC, and ONC treated with MitoTEMPO or Fer-1 rats ($n = 3$ retinas per group). (F, G) Western blot (F) and densitometry analysis (G) of mitochondrial GPx4 expression in control retinas and 6 h, one day, three days and seven days post-ONC ($n = 4$ retinas per group). (H, I) Western blot (I) and densitometry analysis (H) of cytoplasmic GPx4 expression in control and ONC retinas of 6 h, one day, three days and seven days post-ONC ($n = 4$ retinas per group). (J, K) Measurement of retinal mitochondrial (J) and cytoplasmic (K) MDA levels in control and ONC treated retinas at designated time points ($n = 4$ retinas per group). (L, M) Western blot and densitometry analysis of GPx4 expression in control retinas and retinas after three days of ONC treated with normal saline (NS) or MitoTEMPO (Mito) ($n = 3$ retinas per group). (N) Measurement of MDA levels in control eyes and eyes after three days of ONC treated with NS and MitoTEMPO ($n = 3$ retinas per group). (O) Wholemout images of RBPMS-labeled RGCs from control, seven days post-ONC, and ONC treated with NS, Tempo, or MitoTEMPO eyes. (P) Quantification of RBPMS⁺ RGCs shown in (O) ($n = 5-6$ retinas per group). (Q) Representative OCT images of retinas from control, 14 days post-ONC, and ONC treated with NS, Tempo, or MitoTEMPO. (R) Quantification of the mean RNFL thickness shown in (Q) ($n = 6-8$ retinas per group). The data represent the mean \pm SD. * $P < 0.05$, ** $P < 0.01$, and *** $P < 0.001$. Scale bars, 50 μ m in (A) and 200 μ m in (O).

necrosis can only partially rescue RGC loss in these models, suggesting that another form of cell death is involved in optic nerve damage-induced RGC injury [13,53]. In addition, substantial evidence indicates that lipid peroxidation and disturbed iron metabolism are crucial in RGC injury under these conditions. For example, MDA accumulation has been found in the retinas of a rat ONC model and the plasma of patients with primary open-angle glaucoma [54,55]. Similarly, increased mRNA and protein expression of iron-regulating proteins, such as transferrin and ferritin, are present in the retinas of experimental monkey glaucoma and human glaucoma [56]. Moreover, Sakamoto et al. reported a protective effect of iron-chelating agents against MDA-induced RGC loss in rats [43]. In the current study, we demonstrated ferroptosis induction in an ONC rat model and an experimental glaucoma mouse model. In addition, the lipid ROS scavenger Fer-1 effectively promoted RGC survival and restored visual function in ONC retinas, highlighting the significance of ferroptosis in optic nerve axotomy-induced RGC injury. Similarly, Fer-1 treatment also restored the downregulation of GPx4 levels and prevented RGC death and retinal structural impairment caused by IOP elevation in mice, implicating ferroptosis in glaucoma-induced RGC injuries.

To investigate the relative contributions of ferroptosis and apoptosis in ONC-induced RGC injury, the time points at which the two forms of RCDs were induced were examined. We found that the expression of CC3, the executor of apoptosis, was upregulated three days after ONC, while reduced GPx4 protein levels and MDA accumulation were observed as early as 6 h after ONC injury, suggesting that ferroptosis is likely to be an early event in ONC models. Furthermore, we found that applying Fer-1 before ONC did not prevent caspase 3 activation at later time points, suggesting that ferroptosis is induced independently of apoptosis in ONC retinas. Next, we compared the therapeutic efficacy of ferroptosis and apoptosis inhibitors in ONC models and found that the ferroptosis inhibitor Fer-1 exerted a protective effect comparable to that of the apoptosis inhibitor Z-VAD-FMK. The combination of both inhibitors showed a moderate but significantly improved protective effect in rescuing RGC numbers. These results suggest that ferroptosis, along with apoptosis, represents the major form of RCD in RGC death in ONC rat models.

The organelle that triggers ferroptosis remains unclear. Previous studies have reported the generation of lipid peroxides in cells undergoing ferroptosis in the plasma membrane, lysosomes, and endoplasmic reticulum [27,57–62]. Although morphological alterations in mitochondria are characteristic of ferroptosis, whether mitochondrial lipid peroxides are an important component in ferroptosis remains controversial. Previous studies have shown that erastin and RAS-selective lethal (RSL3) can induce ferroptosis without mitochondrial dysfunction or lipid peroxidation [27,63]. In contrast, Gao et al. showed that mitochondrial respiration is required for lipid ROS generation to drive cysteine deprivation-induced ferroptosis [64]. More recently, two studies showed that excessive lipid peroxidation in mitochondria leads to ferroptosis as a major mechanism in doxorubicin (DOX)-induced cardiomyopathy [50,51]. In our study, ferroptosis induction in the ONC retina was accompanied by mitochondrial dysfunction, as manifested by

increased mitochondrial ROS production, decreased ATP production, and the downregulation of mitochondrial genes. Furthermore, GPx4 downregulation and increased MDA accumulation in the mitochondrial fraction of the retina after ONC indicated that lipid ROS generation from dysfunctional mitochondria may trigger ferroptosis in the ONC retina. Hence, we used MitoTEMPO to scavenge ROS in mitochondria and found that MitoTEMPO effectively abolished the reduction of GPx4 expression and MDA accumulation in the ONC retina. Moreover, the MitoTEMPO treatment significantly improved RGC survival and preserved retinal thickness after ONC, supporting a key role of mitochondrial ROS in ONC-induced ferroptosis and RGC death. Due to the high metabolic activity and energy demand, the retina contains a great concentration of mitochondria, especially in RGCs, making them particularly susceptible to perturbations in mitochondrial function [65]. Therefore, mitochondrial dysfunction has been implicated in RGC loss in glaucomatous injury, and targeting mitochondria might be a promising neuroprotective strategy under these conditions [66].

Our study has limitations to be considered. Firstly, we showed the involvement of ferroptosis and the therapeutic potential of anti-ferroptosis reagents in ONC induced acute axonal injury model and microbead occlusion induced glaucoma model, further studies are needed to examine the role of ferroptosis in other experimental and genetic mouse models of glaucoma. Secondly, our data suggest increased mitochondria ROS and lipid peroxides as the principal driver of ferroptosis in ONC retinas, nonetheless, we find that TEMPO, a non-mitochondria targeted antioxidant, also exerts some protective effect in preventing RGC death in ONC models, suggesting that the lipid peroxidation in lipid membranes after ONC may also play a role here. Further investigation is needed to completely decipher the underlying molecular mechanisms of mitochondria dependent ferroptosis in these diseases. Lastly, our findings have not been confirmed in human clinical specimens and future studies using vitreous fluid or retinal sample from optic nerve injury and glaucoma patients are needed to demonstrate the occurrence and significance of ferroptosis in these disease conditions.

In summary, our study revealed a novel mechanism by which mitochondria-dependent ferroptosis mediates RGC death after optic nerve damage, potentially uncovering new therapeutic targets for reducing RGC degeneration in optic neuropathies.

4. Materials and methods

4.1. Animals

Adult male Wistar rats (weighing 180–200 g) and male C57BL/6J mice (6–8 weeks) were purchased from Beijing Vital River Laboratory Animal Technology Co., Ltd. and maintained under a controlled temperature and illumination (12:12 h light: dark cycle). All experimental procedures were approved by the Tianjin Medical University Animal Care and Use Committee.

4.2. ONC

Anesthesia was induced using 5% isoflurane/1.5 L per minute O₂ and maintained at 3% throughout the procedure. Intraorbital ONC was performed as previously described [67]. Briefly, the optic nerve was surgically exposed intraorbitally and crushed using reverse microscopic self-closing forceps (Dumont #N7, Cat #RS-5027, Roboz, Montignez, Switzerland) for 10 s 1.5 mm posterior to the optic disc. Care was taken to avoid damaging the retinal artery during the procedure.

4.3. Mouse model of elevated IOP by microbead injection

C57BL/6J mice were anesthetized with 3% isoflurane/1.5 L per minute O₂ and maintained at 3% throughout the procedure. Elevation of IOP was induced unilaterally by injection of polystyrene microbeads (FluoSpheres, 15 μm diameter, Invitrogen, CA, USA) into the anterior chamber of each animal under a surgical microscope, as previously reported [48]. Briefly, microbeads were prepared at a concentration of 5.0 × 10⁶ beads/mL in sterile physiological saline. A *trans*-corneal incision was made near the center using an insulin syringe with a sterile interior (Becton, Dickinson and Company, NJ, USA). Then, 2 μL of microbeads was injected into the anterior chamber through the incision and an air bubble was injected to prevent leakage using a 33G-Hamilton syringe (World Precision Instruments Inc., FL, USA). Animals were excluded for symptoms of inflammation (clouding and edema of the cornea). IOP was monitored by a rebound TonoLab tonometer (ICARE, Finland). IOP readings were reported as the average of six consecutive IOP measurements. All IOPs were measured between 10:00 a.m. and 12:00 a.m. of the day.

4.4. Intraocular injection

A 5 μL Hamilton syringe with a 33G needle was used for intravitreal injection, and care was taken during the injection to avoid damage to the lens of the animals. Wistar rats received 4 μL of Fer-1 (10 μM or 1 mM) (Cat#S7243, Selleck, TX, USA), Z-VAD-FMK (400 ng) (Cat#S7023, Selleck), Tempo (2 mM) (Cat#176141, Sigma, Darmstadt, Germany), and MitoTEMPO (2 mM) (Cat#SML0737, Sigma) injected into the vitreous cavity before and three days after ONC injury. For C57BL/6J mice, 2 μL of Fer-1 (1 mM) was injected into the vitreous cavity immediately before the microbeads were injected into the anterior chamber. Fer-1 was dissolved in 0.1% dimethyl sulfoxide (DMSO). [Supplemental Fig. 1](#) shows the safety evaluation of the intravitreal Fer-1 injection.

4.5. Western blot

Retinal tissue was lysed in radioimmunoprecipitation assay (RIPA) buffer containing protease inhibitors (APExBIO, TX, USA). The extracted proteins were separated on 15% sodium dodecyl sulfate-polyacrylamide gels (SDS-PAGE) and transferred to polyvinylidene difluoride (PVDF) membranes (Merck Millipore, Darmstadt, Germany). After blocking with 5% skim milk, the membranes were incubated at 4 °C overnight with the following primary antibodies: GPx4 (1:1000, Cat#ab125066, Abcam, Cambridge, UK), xCT (1:1000, Cat#ab175186, Abcam), CC3 (1:500, Cat#9664, Cell Signaling Technology, MA, USA), Cyto C (1:1000, Cat#11940S, Cell Signaling Technology), COX IV (1:1000, Cat#4844, Cell Signaling Technology), and glyceraldehyde-3-phosphate dehydrogenase (GAPDH) (1:5000, UtiBody, Tianjin, China). The membranes were washed and incubated with secondary antibodies for 2 h at room temperature. The blots were detected using an automatic chemiluminescence analysis system (Millipore, Billerica, MA, USA). The blots were quantified using ImageJ software.

4.6. RNA extraction and quantitative real-time PCR (qRT-PCR) analysis

Total RNA was extracted from the retinas using TRIzol® reagent

(Sigma) and converted to complementary DNA (cDNA) using reverse transcriptase (TransGen, Beijing, China). qRT-PCR was performed using PerfectStart® Green qPCR SuperMix (TransGen) and processed with a 7500 Real-Time PCR system (Applied Biosystems, CA, US). All samples were normalized to β-actin levels. Relative mRNA levels were quantified using the ΔΔCt method. The primers used in this study were as follows: *MT-ATP6* forward, 5'-GAACGCCTAATCAGCAAC-3'; *MT-ATP6* reverse, 5'-AATGTATGGGGAAGAAGC-3'; *mt-Cytb* forward, 5'-CCCATTTCATATCGCCGC-3'; *mt-Cytb* reverse, 5'-GGGTGTTGAGGGGTTAGC-3'; *GPx4* forward, 5'-AATCCTGGCCTTCCCTTGCA-3'; *GPx4* reverse, 5'-GCCCTTGGGCTGGACTTTCA-3'; *β-actin* forward, 5'-GATCAAGATCATTGCTCCTCTG-3'; *β-actin* reverse, 5'-ACGCAGCTCAGTAA-CAGTCC-3'.

4.7. Analyzing oxylipins

Oxylipins were analyzed using UHPLC-MS/MS with an Ultimate 3000 UHPLC system (ThermoFisher, MA, USA) connected to a Q Exactive™ Hybrid Quadrupole-Orbitrap™ Mass Spectrometer (QE) (ThermoFisher, MA, USA) equipped with an electrospray ion source. Lipids were separated using an ACQUITY UPLC CSH C18 column (2.1 mm × 100 mm, 1.7 μm) (Waters, MA, USA) with a column temperature of 55 °C. Internal standards were purchased from Avanti Polar Lipids Inc.

4.8. Quantification of RGC survival

Eyeballs were removed and fixed in 4% paraformaldehyde (PFA) for 2 h at room temperature, followed by isolation and permeabilization with 1% Triton X-100 (Solarbio, Beijing, China) and blocking in 5% albumin bovine V (Solarbio) and 0.5% Triton X-100. Next, retinal wholemounts were incubated with an *anti*-RBPMS antibody (1:200, Cat#ab152101, Abcam) at 4 °C for two days, washed six times with 0.1% Triton X-100, then incubated with anti-rabbit Alexa Fluor 488 (1:200, Cat#111-545-003, Jackson Immuno Research, PA, USA) for 2 h, protected from light. After washing, the retinal wholemounts were scanned using a Zeiss LSM800 confocal microscope (Zeiss, Munich, Germany). RGC quantification was performed using ImageJ software by counting RBPMS⁺ cells from 3 mm-square areas per retinal quadrant at distances of 0.5 mm, 1.5 mm, and 2.5 mm for rats or 0.25 mm, 0.75 mm, and 1.25 mm for mice from the optic nerve head for a total of 12 retinal areas.

4.9. F-VEP recording

F-VEP was performed using an RETI-port/scan 21 vision electrophysiological diagnostic instrument (Roland Consult, Brandenburg, Germany) as previously described [67]. Wistar rats were anesthetized intraperitoneally with 10% chloral hydrate (300 mg/kg) and were dark-adapted for 15 min in a dark room. Three silver needle electrodes were used, with the recording electrode placed subcutaneously in the middle of two ears, the reference electrode hooked into the cheek on the side of the measured eye, and the ground electrode placed under the skin of the tail. The other eye was covered with a piece of black cloth while one eye was being tested. The test parameters were as follows: the intensity of the white flash stimulus was 3.0 cd²/m², the stimulation frequency was 1.4 Hz, and each item was superimposed 100 times. We detected the latency of the N1 and P1 waves and the amplitudes of N1–P1 (from the N1 trough to the P1 peak) and P1–N2 (from the P1 peak to the N2 trough).

4.10. Spectral-domain optical coherence tomography (SD-OCT) imaging

After intraperitoneal anesthesia with 10% chloral hydrate (300 mg/kg), the rats were treated with atropine eye drops for 5–10 min to dilate the pupils. A drop of ofloxacin eye ointment was applied to each cornea to prevent dryness. The images of the rat retinas were scanned in the ring

scan mode centered by the optic nerve head using a Phoenix Micron IV retinal imaging microscope (Phoenix, OR, USA), and 20 images at the same position were averaged to eliminate artifacts. The Phoenix software quantified the average thickness of the RNFL around the optic nerve head.

4.11. TEM

After sacrificing the subjects, eyeballs were quickly removed and fixed in 2.5% glutaraldehyde (Solarbio) for 2–4 h. Then the retina-choroid-sclera complex was dissected, cut into small 1 mm³ clumps, post-fixed with 1% osmium tetroxide in a 0.1 M phosphate buffer (PB, pH 7.4) at room temperature for 2 h, dehydrated in a graded ethyl alcohol series, and embedded in SPI-Pon 812 epoxy resin (SPI, Cat#90529-77-4, PA, USA) overnight at 37 °C. The embedded tissues were polymerized for more than 48 h at 60 °C. Then 60–80 nm ultra-thin sections were cut using a Leica UC7 ultramicrotome, stained with 2% uranium acetate saturated alcohol solution for 8 min and 2.6% lead citrate for 8 min, and observed under an HT7700 transmission electron microscope (HITACHI, Tokyo, Japan).

4.12. Measuring MDA and tissue iron levels

Retinal MDA and iron levels in homogenized retinal tissues were determined using an MDA assay kit (cat#A003-1-2, Nanjing Jiancheng Bioengineering Institute, Nanjing, China) and a tissue iron assay kit (cat#A039-2-1, Nanjing Jiancheng Bioengineering Institute). Briefly, MDA levels were determined by measuring the optical density (OD) at 532 nm and iron levels at 520 nm using a microplate reader (Biotek, VT, USA). MDA and iron levels were normalized to the total protein levels determined using a bicinchoninic acid (BCA) assay (Solarbio).

4.13. Isolating cytosolic and mitochondrial fractions

Cytosolic and mitochondrial fractions were isolated using fresh retinal tissues and a mitochondria isolation kit (cat#G006-1-1, Nanjing Jiancheng Bioengineering Institute) per the manufacturer's instructions.

4.14. Detecting ATP levels

ATP content was determined using an enhanced ATP assay kit (cat#S0027, Beyotime, Shanghai, China) per the manufacturer's instructions. Briefly, retinal tissues were lysed and homogenized with 150 µL cold lysis buffer on ice and centrifuged at 12 000 g at 4 °C for 10 min. The ATP detection solution (100 µL) was added to a 96-well plate and incubated at room temperature for 5 min. Then a 20 µL supernatant of the retinal lysate was transferred into a 96-well plate, mixed quickly, and read after 2 s of incubation with the ATP detection solution using a microplate reader (Biotek). Total ATP levels were calculated from luminescence signals and normalized to protein concentrations.

4.15. Detecting total ROS and mitochondria-derived ROS

Total and mitochondria-derived ROS in the retina were measured using CellROX™ Green (cat#C10444, Thermo Fisher Scientific) and Mitosox™ Red (cat#M36008, Thermo Fisher Scientific). Briefly, 4 µL of Mitosox and 4 µL of CellROX at a concentration of 250 µM were intravitreally injected into Wistar rats 2 h before sacrifice. The eyeballs were harvested and fixed with 4% PFA on ice for 1 h and protected from light. Eyecups were dissected and cryosectioned into 20 µm sections onto glass slides, washed with phosphate-buffered saline (PBS), and mounted in mounting medium containing 4',6-diamidino-2-phenylindole (DAPI) (Invitrogen). Fluorescence signals were evaluated using a confocal microscope (LSM 800; Carl Zeiss, Jena, Germany).

4.16. Laser capture microdissection of RGCs

Eyeballs from ONC and control rats were embedded in OCT immediately after enucleation, cut into 8 µm sections, and collected on polyethylene naphthalate membrane slides (Zeiss, Munich, Germany), which were rinsed in 0.1% diethyl pyrocarbonate (DEPC). The sections were thawed at room temperature for 2 min, rinsed briefly in 0.1% DEPC, and subjected to HE staining with hematoxylin for 10 s and eosin for 5 s, with a brief rinsing with 0.1% DEPC between each step. Then, the sections were dehydrated with 50%, 70%, 95%, and 100% ethanol and air-dried. All processes were performed on ice, and all steps were prepared in 0.1% DEPC. Cells with large round or oval nuclei in the RGC layer were microdissected via laser pressure catapulting using a Palm Zeiss UV laser capture microdissection system (Palm Zeiss Microlaser Technologies, Munich, Germany). RNA was extracted from microdissected RGCs using an RNeasy Micro Kit (cat#74004; Qiagen, Hilden, Germany), and real-time PCR was performed.

4.17. Statistical analysis

Quantitative results are presented as the mean ± SD. The statistical significance of differences was analyzed using a Student's *t*-test between two groups or a one-way analysis of variance (ANOVA) among at least three groups. Statistical significance was set at *P* < 0.05. All statistical analyses were performed using Prism 8.0.2 (GraphPad Software, San Diego, CA, USA).

Ethics statement

All animal experiments were conducted in accordance with the guidelines of the Tianjin Medical University Animal Ethics and Welfare Committee (TMUaMEC 2020003).

Funding statement

This work was supported by the National Natural Science Foundation of China (Grant Number 82020108007, 82101131, 32171101, 82122018,81900882).

Author contribution statement

M.G., H.-Y., M.D., and X.W. conceived the project and designed the experiments. M.G., Y.Z., Y.-S., X.M., and X.D. conducted the experiments. Y.Z., H.Z., and S.H. performed the data analysis. M.D., M.G., and Y.Z. drafted and revised the manuscript. H.Y., M.D., and X.W. supervised the study. All authors have read and approved the final manuscript.

Declaration of competing interest

The authors declare no conflict of interest.

Data availability

Data will be made available on request.

Acknowledgements

None.

Appendix A. Supplementary data

Supplementary data to this article can be found online at <https://doi.org/10.1016/j.redox.2022.102541>.

References

- [1] T. Baden, P. Berens, K. Franke, M. Roman Roson, M. Bethge, T. Euler, The functional diversity of retinal ganglion cells in the mouse, *Nature* 529 (7586) (2016) 345–350, <https://doi.org/10.1038/nature16468>.
- [2] R.H. Masland, The neuronal organization of the retina, *Neuron* 76 (2) (2012) 266–280, <https://doi.org/10.1016/j.neuron.2012.10.002>.
- [3] R.S. Khan, A.G. Ross, P. Aravand, K. Dine, E.B. Selzer, K.S. Shindler, RGC and vision loss from traumatic optic neuropathy induced by repetitive closed head trauma is dependent on timing and force of impact, *Transl. Vis. Sci. Technol.* 10 (1) (2021) 8, <https://doi.org/10.1167/tvst.10.1.8>.
- [4] O.W. Gramlich, C.R. Godwin, N.D. Heuss, D.S. Gregerson, M.H. Kuehn, T and B Lymphocyte deficiency in Rag1^{-/-} mice reduces retinal ganglion cell loss in experimental glaucoma, *Invest. Ophthalmol. Visual Sci.* 61 (14) (2020) 18, <https://doi.org/10.1167/iovs.61.14.18>.
- [5] B. Laha, B.K. Stafford, A.D. Huberman, Regenerating optic pathways from the eye to the brain, *Science* 356 (6342) (2017) 1031–1034, <https://doi.org/10.1126/science.aal5060>.
- [6] S. Isenmann, A. Kretz, A. Cellerino, Molecular determinants of retinal ganglion cell development, survival, and regeneration, *Prog. Retin. Eye Res.* 22 (4) (2003) 483–543, [https://doi.org/10.1016/s1350-9462\(03\)00027-2](https://doi.org/10.1016/s1350-9462(03)00027-2).
- [7] L.A. Mesentier-Louro, P. Rosso, V. Carito, R. Mendez-Otero, M.F. Santiago, P. Rama, et al., Nerve growth factor role on retinal ganglion cell survival and axon regrowth: effects of ocular administration in experimental model of optic nerve injury, *Mol. Neurobiol.* 56 (2) (2019) 1056–1069, <https://doi.org/10.1007/s12035-018-1154-1>.
- [8] L. Feng, Z. Puyang, H. Chen, P. Liang, J.B. Troy, X. Liu, Overexpression of brain-derived neurotrophic factor protects large retinal ganglion cells after optic nerve crush in mice, *eNeuro* 4 (1) (2017), <https://doi.org/10.1523/ENEURO.0331-16.2016>.
- [9] X.X. Fan, Z.Y. Cao, M.X. Liu, W.J. Liu, Z.L. Xu, P.F. Tu, et al., Diterpene Ginkgolides Meglumine injection inhibits apoptosis induced by optic nerve crush injury via modulating MAPKs signaling pathways in retinal ganglion cells, *J. Ethnopharmacol.* 279 (2021), 114371, <https://doi.org/10.1016/j.jep.2021.114371>.
- [10] X. Jiao, Y. Peng, L. Yang, Minocycline protects retinal ganglion cells after optic nerve crush injury in mice by delaying autophagy and upregulating nuclear factor-kappaB2, *Chin. Med. J.* 127 (9) (2014) 1749–1754.
- [11] Z. Qijun, Z. Huan, G. Ling, C. Kaijian, L. Wei, J. Shuxing, et al., The levels and significance of inflammases in the mouse retina following optic nerve crush, *Int. Immunopharm.* 71 (2019) 313–320, <https://doi.org/10.1016/j.intimp.2019.03.029>.
- [12] N. Rodriguez-Muela, F. Germain, G. Marino, P.S. Fitze, P. Boya, Autophagy promotes survival of retinal ganglion cells after optic nerve axotomy in mice, *Cell Death Differ.* 19 (1) (2012) 162–169, <https://doi.org/10.1038/cdd.2011.88>.
- [13] M. Fitzgerald, S.C. Payne, C.A. Bartlett, L. Evill, A.R. Harvey, S.A. Dunlop, Secondary retinal ganglion cell death and the neuroprotective effects of the calcium channel blocker lomerizine, *Invest. Ophthalmol. Vis. Sci.* 50 (11) (2009) 5456–5462, <https://doi.org/10.1167/iovs.09-3717>.
- [14] H.Y. Li, Y.W. Ruan, C.R. Ren, Q. Cui, K.F. So, Mechanisms of secondary degeneration after partial optic nerve transection, *Neural Regen Res.* 9 (6) (2014) 565–574, <https://doi.org/10.4103/1673-5374.130093>.
- [15] S.J. McKinnon, Glaucoma, apoptosis, and neuroprotection, *Curr. Opin. Ophthalmol.* 8 (2) (1997) 28–37, <https://doi.org/10.1097/00055735-199704000-00006>.
- [16] X. Zhou, F. Li, L. Kong, H. Tomita, C. Li, W. Cao, Involvement of inflammation, degradation, and apoptosis in a mouse model of glaucoma, *J. Biol. Chem.* 280 (35) (2005) 31240–31248, <https://doi.org/10.1074/jbc.M502641200>.
- [17] L.A. Kerrigan, D.J. Zack, H.A. Quigley, S.D. Smith, M.E. Pease, TUNEL-positive ganglion cells in human primary open-angle glaucoma, *Arch. Ophthalmol.* 115 (8) (1997) 1031–1035, <https://doi.org/10.1001/archoph.1997.01100160201010>.
- [18] M.F. Cordeiro, E.M. Normando, M.J. Cardoso, S. Miodragovic, S. Jeylani, B. M. Davis, et al., Real-time imaging of single neuronal cell apoptosis in patients with glaucoma, *Brain* 140 (6) (2017) 1757–1767, <https://doi.org/10.1093/brain/awx088>.
- [19] P.P. Monnier, P.M. D'Onofrio, M. Magharious, A.C. Hollander, N. Tassew, K. Szydlowska, et al., Involvement of caspase-6 and caspase-8 in neuronal apoptosis and the regenerative failure of injured retinal ganglion cells, *J. Neurosci.* 31 (29) (2011) 10494–10505, <https://doi.org/10.1523/JNEUROSCI.0148-11.2011>.
- [20] J.X. Zhou, Y.J. Liu, X. Chen, X. Zhang, J. Xu, K. Yang, et al., Low-intensity pulsed ultrasound protects retinal ganglion cell from optic nerve injury induced apoptosis via yes associated protein, *Front. Cell. Neurosci.* 12 (2018) 160, <https://doi.org/10.3389/fncel.2018.00160>.
- [21] L. Zuo, R.S. Khan, V. Lee, K. Dine, W. Wu, K.S. Shindler, SIRT1 promotes RGC survival and delays loss of function following optic nerve crush, *Invest. Ophthalmol. Visual Sci.* 54 (7) (2013) 5097–5102, <https://doi.org/10.1167/iovs.13-12157>.
- [22] R. Wang, Q. Sun, F. Xia, Z. Chen, J. Wu, Y. Zhang, et al., Methane rescues retinal ganglion cells and limits retinal mitochondrial dysfunction following optic nerve crush, *Exp. Eye Res.* 159 (2017) 49–57, <https://doi.org/10.1016/j.exer.2017.03.008>.
- [23] Z. Zheng, R. Yuan, M. Song, Y. Huo, W. Liu, X. Cai, et al., The toll-like receptor 4-mediated signaling pathway is activated following optic nerve injury in mice, *Brain Res.* 1489 (2012) 90–97, <https://doi.org/10.1016/j.brainres.2012.10.014>.
- [24] U. Schmitt, B.A. Sabel, MK-801 reduces retinal ganglion cell survival but improves visual performance after controlled optic nerve crush, *J. Neurotrauma* 13 (12) (1996) 791–800, <https://doi.org/10.1089/neu.1996.13.791>.
- [25] E. Yoles, M. Schwartz, Elevation of intracellular glutamate levels in rats with partial lesion of the optic nerve, *Arch. Ophthalmol.* 116 (7) (1998) 906–910, <https://doi.org/10.1001/archoph.116.7.906>.
- [26] F. Schuettauf, R. Naskar, C.K. Vorwerk, D. Zurakowski, E.B. Dreyer, Ganglion cell loss after optic nerve crush mediated through AMPA-kainate and NMDA receptors, *Invest. Ophthalmol. Visual Sci.* 41 (13) (2000) 4313–4316.
- [27] S.J. Dixon, K.M. Lemberg, M.R. Lamprecht, R. Skouta, E.M. Zaitsev, C.E. Gleason, et al., Ferroptosis: an iron-dependent form of nonapoptotic cell death, *Cell* 149 (5) (2012) 1060–1072, <https://doi.org/10.1016/j.cell.2012.03.042>.
- [28] Y. Sun, P. Chen, B. Zhai, M. Zhang, Y. Xiang, J. Fang, et al., The emerging role of ferroptosis in inflammation, *Biomed. Pharmacother.* 127 (2020), 110108, <https://doi.org/10.1016/j.biopha.2020.110108>.
- [29] Y. Xie, W. Hou, X. Song, Y. Yu, J. Huang, X. Sun, et al., Ferroptosis: process and function, *Cell Death Differ.* 23 (3) (2016) 369–379, <https://doi.org/10.1038/cdd.2015.158>.
- [30] N. Kajarabille, G.O. Latunde-Dada, Programmed cell-death by ferroptosis: antioxidants as mitigators, *Int. J. Mol. Sci.* 20 (19) (2019), <https://doi.org/10.3390/ijms20194968>.
- [31] L. Jiang, N. Kon, T. Li, S.J. Wang, T. Su, H. Hibshoosh, et al., Ferroptosis as a p53-mediated activity during tumour suppression, *Nature* 520 (7545) (2015) 57–62, <https://doi.org/10.1038/nature14344>.
- [32] Y. Li, D. Feng, Z. Wang, Y. Zhao, R. Sun, D. Tian, et al., Ischemia-induced ACSL4 activation contributes to ferroptosis-mediated tissue injury in intestinal ischemia/reperfusion, *Cell Death Differ.* 26 (11) (2019) 2284–2299, <https://doi.org/10.1038/s41418-019-0299-4>.
- [33] H. Wang, P. An, E. Xie, Q. Wu, X. Fang, H. Gao, et al., Characterization of ferroptosis in murine models of hemochromatosis, *Hepatology* 66 (2) (2017) 449–465, <https://doi.org/10.1002/hep.29117>.
- [34] W.S. Hambricht, R.S. Fonseca, L. Chen, R. Na, Q. Ran, Ablation of ferroptosis regulator glutathione peroxidase 4 in forebrain neurons promotes cognitive impairment and neurodegeneration, *Redox Biol.* 12 (2017) 8–17, <https://doi.org/10.1016/j.redox.2017.01.021>.
- [35] B. Do Van, F. Gouel, A. Jonneaux, K. Timmerman, P. Gele, M. Petraut, et al., Ferroptosis, a newly characterized form of cell death in Parkinson's disease that is regulated by PKC, *Neurobiol. Dis.* 94 (2016) 169–178, <https://doi.org/10.1016/j.nbd.2016.05.011>.
- [36] K. Totsuka, T. Ueta, T. Uchida, M.F. Roggia, S. Nakagawa, D.G. Vavvas, et al., Oxidative stress induces ferroptotic cell death in retinal pigment epithelial cells, *Exp. Eye Res.* 181 (2019) 316–324, <https://doi.org/10.1016/j.exer.2018.08.019>.
- [37] Tang W, Guo J, Liu W, Ma J, Xu G. Ferrostatin-1 attenuates ferroptosis and protects the retina against light-induced retinal degeneration. *Biochem. Biophys. Res. Commun.*, 548 (2021):27-34 doi: 10.1016/j.bbrc.2021.02.055.
- [38] X. Zhao, M. Gao, J. Liang, Y. Chen, Y. Wang, Y. Wang, et al., SLC7A11 reduces laser-induced choroidal neovascularization by inhibiting RPE ferroptosis and VEGF production, *Front. Cell Dev. Biol.* 9 (2021), 639851, <https://doi.org/10.3389/fcell.2021.639851>.
- [39] D.M. Inman, W.S. Lambert, D.J. Calkins, P.J. Horner, alpha-Lipoic acid antioxidant treatment limits glaucoma-related retinal ganglion cell death and dysfunction, *PLoS One* 8 (6) (2013), e65389, <https://doi.org/10.1371/journal.pone.0065389>.
- [40] B. Chhunchha, P. Singh, W.D. Stamer, D.P. Singh, Prdx6 retards senescence and restores trabecular meshwork cell health by regulating reactive oxygen species, *Cell Death Dis.* 3 (2017), 17060, <https://doi.org/10.1038/cddiscovery.2017.60>.
- [41] E.M. McElnea, B. Quill, N.G. Docherty, M. Imratan, W.F. Siah, A.F. Clark, et al., Oxidative stress, mitochondrial dysfunction and calcium overload in human lamina cribrosa cells from glaucoma donors, *Mol. Vis.* 17 (2011) 1182–1191.
- [42] Y. Zhao, S. Wang, C.M. Sorenson, L. Teixeira, R.R. Dubielzig, D.M. Peters, et al., Cyp11b mediates periostin regulation of trabecular meshwork development by suppression of oxidative stress, *Mol. Cell Biol.* 33 (21) (2013) 4225–4240, <https://doi.org/10.1128/mcb.00856-13>.
- [43] K. Sakamoto, T. Suzuki, K. Takahashi, T. Koguchi, T. Hirayama, A. Mori, et al., Iron-chelating agents attenuate NMDA-induced neuronal injury via reduction of oxidative stress in the rat retina, *Exp. Eye Res.* 171 (2018) 30–36, <https://doi.org/10.1016/j.exer.2018.03.008>.
- [44] B.S. Xie, Y.Q. Wang, Y. Lin, Q. Mao, J.F. Feng, G.Y. Gao, et al., Inhibition of ferroptosis attenuates tissue damage and improves long-term outcomes after traumatic brain injury in mice, *CNS Neurosci. Ther.* 25 (4) (2019) 465–475, <https://doi.org/10.1111/cns.13069>.
- [45] G. Miotto, M. Rossetto, M.L. Di Paolo, L. Orian, R. Venerando, A. Roveri, et al., Insight into the mechanism of ferroptosis inhibition by ferrostatin-1, *Redox Biol.* 28 (2020), 101328, <https://doi.org/10.1016/j.redox.2019.101328>.
- [46] N. Li, W. Wang, H. Zhou, Q. Wu, M. Duan, C. Liu, et al., Ferritinophagy-mediated ferroptosis is involved in sepsis-induced cardiac injury, *Free Radic. Biol. Med.* 160 (2020) 303–318, <https://doi.org/10.1016/j.freeradbiomed.2020.08.009>.
- [47] G. Akiyama, Y. Azuchi, X. Guo, T. Noro, A. Kimura, C. Harada, et al., Edaravone prevents retinal degeneration in adult mice following optic nerve injury, *Invest. Ophthalmol. Visual Sci.* 58 (11) (2017) 4908–4914, <https://doi.org/10.1167/iovs.17-22250>.
- [48] Y. Lu, B. Brommer, X. Tian, A. Krishnan, M. Meer, C. Wang, et al., Reprogramming to recover youthful epigenetic information and restore vision, *Nature* 588 (7836) (2020) 124–129, <https://doi.org/10.1038/s41586-020-2975-4>.
- [49] A. Krishnan, A.J. Kocab, D.N. Zacks, A. Marshak-Rothstein, M. Gregory-Ksander, A small peptide antagonist of the Fas receptor inhibits neuroinflammation and prevents axon degeneration and retinal ganglion cell death in an inducible mouse

- model of glaucoma, *J. Neuroinflammation* 16 (1) (2019) 184, <https://doi.org/10.1186/s12974-019-1576-3>.
- [50] T. Tadokoro, M. Ikeda, T. Ide, H. Deguchi, S. Ikeda, K. Okabe, et al., Mitochondria-dependent ferroptosis plays a pivotal role in doxorubicin cardiotoxicity, *JCI insight* 5 (9) (2020), <https://doi.org/10.1172/jci.insight.132747>.
- [51] X. Fang, H. Wang, D. Han, E. Xie, X. Yang, J. Wei, et al., Ferroptosis as a target for protection against cardiomyopathy, *Proc. Natl. Acad. Sci. U.S.A.* 116 (7) (2019) 2672–2680, <https://doi.org/10.1073/pnas.1821022116>.
- [52] R.N. Weinreb, T. Aung, F.A. Medeiros, The pathophysiology and treatment of glaucoma: a review, *JAMA* 311 (18) (2014) 1901–1911, <https://doi.org/10.1001/jama.2014.3192>.
- [53] R. Huang, Q. Lan, L. Chen, H. Zhong, L. Cui, L. Jiang, et al., Attenuates retinal glial responses and RGCs apoptosis after optic nerve crush by modulating CD200/CD200R1 interaction, *CD200Fc*, *J. Mol. Neurosci.* 64 (2) (2018) 200–210, <https://doi.org/10.1007/s12031-017-1020-z>.
- [54] J.C. Sun, T. Xu, Q. Zuo, R.B. Wang, A.Q. Qi, W.L. Cao, et al., Hydrogen-rich saline promotes survival of retinal ganglion cells in a rat model of optic nerve crush, *PLoS One* 9 (6) (2014), e99299, <https://doi.org/10.1371/journal.pone.0099299>.
- [55] O. Yildirim, N.A. Ates, B. Ercan, N. Muslu, A. Unlu, L. Tamer, et al., Role of oxidative stress enzymes in open-angle glaucoma, *Eye* 19 (5) (2005) 580–583, <https://doi.org/10.1038/sj.eye.6701565>.
- [56] R.H. Farkas, I. Chowers, A.S. Hackam, M. Kageyama, R.W. Nickells, D.C. Otteson, et al., Increased expression of iron-regulating genes in monkey and human glaucoma, *Invest. Ophthalmol. Vis. Sci.* 45 (5) (2004) 1410–1417, <https://doi.org/10.1167/iovs.03-0872>.
- [57] B. Yan, Y. Ai, Q. Sun, Y. Ma, Y. Cao, J. Wang, et al., Membrane damage during ferroptosis is caused by oxidation of phospholipids catalyzed by the oxidoreductases POR and CYB5R1, *Mol. Cell.* 81 (2) (2021) 355–369, <https://doi.org/10.1016/j.molcel.2020.11.024>, e310.
- [58] Y. Hirata, Y. Tsunekawa, M. Takahashi, K. Oh-Hashi, K. Kawaguchi, M. Hayazaki, et al., Identification of novel neuroprotective N,N-dimethylaniline derivatives that prevent oxytosis/ferroptosis and localize to late endosomes and lysosomes, *Free Radic. Biol. Med.* 174 (2021) 225–235, <https://doi.org/10.1016/j.freeradbiomed.2021.08.015>.
- [59] J. Wen, H. Chen, Z. Ren, P. Zhang, J. Chen, S. Jiang, Ultrasmall iron oxide nanoparticles induced ferroptosis via Beclin1/ATG5-dependent autophagy pathway, *Nano Converge* 8 (1) (2021) 10, <https://doi.org/10.1186/s40580-021-00260-z>.
- [60] Zhao C, Yu D, He Z, Bao L, Feng L, Chen L, et al. Endoplasmic reticulum stress-mediated autophagy activation is involved in cadmium-induced ferroptosis of renal tubular epithelial cells. *Free Radic. Biol. Med.*, 175 (2021):236-248 doi: 10.1016/j.freeradbiomed.2021.09.008.
- [61] V.E. Kagan, G. Mao, F. Qu, J.P. Angeli, S. Doll, C.S. Croix, et al., Oxidized arachidonic and adrenic PES navigate cells to ferroptosis, *Nat. Chem. Biol.* 13 (1) (2017) 81–90, <https://doi.org/10.1038/nchembio.2238>.
- [62] S. Torii, R. Shintoku, C. Kubota, M. Yaegashi, R. Torii, M. Sasaki, et al., An essential role for functional lysosomes in ferroptosis of cancer cells, *Biochem. J.* 473 (6) (2016) 769–777, <https://doi.org/10.1042/BJ20150658>.
- [63] J.P. Friedmann Angeli, M. Schneider, B. Proneth, Y.Y. Tyurina, V.A. Tyurin, V. J. Hammond, et al., Inactivation of the ferroptosis regulator Gpx4 triggers acute renal failure in mice, *Nat. Cell Biol.* 16 (12) (2014) 1180–1191, <https://doi.org/10.1038/ncb3064>.
- [64] M. Gao, J. Yi, J. Zhu, A.M. Minikes, P. Monian, C.B. Thompson, et al., Role of mitochondria in ferroptosis, *Mol. Cell.* 73 (2) (2019) 354–363, <https://doi.org/10.1016/j.molcel.2018.10.042>, e353 doi:.
- [65] G.Y. Kong, N.J. Van Bergen, I.A. Trounce, J.G. Crowston, Mitochondrial dysfunction and glaucoma, *J. Glaucoma* 18 (2) (2009) 93–100, <https://doi.org/10.1097/IJG.0b013e318181284f>.
- [66] P.A. Williams, J.M. Harder, N.E. Foxworth, K.E. Cochran, V.M. Philip, V. Porciatti, et al., Vitamin B3 modulates mitochondrial vulnerability and prevents glaucoma in aged mice, *Science* 355 (6326) (2017) 756–760, <https://doi.org/10.1126/science.aal0092>.
- [67] T. Wang, Y. Li, M. Guo, X. Dong, M. Liao, M. Du, et al., Exosome-Mediated delivery of the neuroprotective peptide PACAP38 promotes retinal ganglion cell survival and axon regeneration in rats with traumatic optic neuropathy, *Front. Cell Dev. Biol.* 9 (2021), 659783, <https://doi.org/10.3389/fcell.2021.659783>.